A Quasi-linear Eddy-Viscosity Model for the Flux of Energy and Momentum to Wind Waves Using Conservation-Law Equations in a Curvilinear Coordinate System

ALASTAIR D. JENKINS

IBM Bergen Scientific Centre, Bergen, Norway

(Manuscript received 19 March 1991, in final form 21 October 1991)

ABSTRACT

The airflow above ocean waves is calculated using a quasi-linear model—one in which the effect of the waves on the mean flow is taken into account. The model uses curvilinear coordinates, in which one coordinate surface coincides with the instantaneous sea surface, and is consequently able to attain fine vertical resolution in the boundary layer just above the sea surface; the model equations are formulated in conservation-law form. The rates of energy and momentum input to the wave field are calculated from the oscillatory pressure and shear-stress components at the water surface. The equations are solved iteratively using a logarithmically spaced finite-difference mesh.

The effect of air turbulence is modeled using a vertically varying shear-stress–dependent eddy viscosity, which acts on the wave-correlated oscillatory motions as well as on the mean flow field. For infinitesimal waves the model agrees with the results of Conte and Miles as the Newtonian viscosity and eddy viscosity that act on the oscillatory motions are reduced toward zero, and it converges slowly toward the results of Jacobs' analytical eddy viscosity model as the drag coefficient is reduced.

In agreement with results from Janssen's simpler quasi-linear model, there is increased wave-induced drag for young wind seas with unidirectional JONSWAP spectra and Phillips constant proportional to the $(-3/2)$ power of wave age. The present model gives similar values for wave drag and wave energy input to Janssen's, for the same values of roughness length and Phillips constant, and the spectral distribution of the rate of energy input to the waves is also in reasonable agreement. The variation of drag coefficient with wave age is quite close to the results obtained by Maat, Kraan, and Oost from analysis of HEXMAX field data.

1. Introduction

The air–sea flux of momentum and mechanical energy has considerable relevance to weather conditions and climate, as well as to the local evolution of ocean waves and currents. Surface gravity waves are a very energetic component of the processes that occur at the atmosphere–ocean interface and, as such, have a strong influence on fluxes across the interface, as well as being of major practical importance to navigation, coastal protection, and offshore engineering operations.

Waves, being irregularities on the sea surface, obviously influence the air–sea momentum flux. Since waves have momentum, the growth of waves by wind action will lead to part of the air–sea momentum flux going into waves (Stewart 1961, 1974), where it can be transported horizontally relatively rapidly (at the wave group velocity) before being transferred to ocean currents as the waves dissipate. The effect of waves on the air–sea flux of momentum is a major focus of attention in this paper, and leads us to consider the effect of wind, that is, the airflow over waves, in making waves grow.

Probably the most important mechanism for wave growth and atmosphere-to-wave energy flux is the "sheltering" mechanism of Jeffreys (1925), developed further by Miles (1957, 1959, 1960). It is certainly very widely used in wave forecasting models (e.g., The SWAMP Group 1985). The airflow over a wavy sea surface induces a pressure fluctuation, proportional to the wave amplitude, which is partly in phase with the sea surface slope and which tends to feed energy into the waves. Miles (1957) predicted that this pressure fluctuation should be approximately proportional to the "curvature" of the wind velocity profile, $(d^2U/dz^2)/[(dU/dz)^3]$, evaluated at the critical height $z = z_c$ where the wind speed U is equal to the wave phase speed. Jeffreys also considered an alternative skin-friction mechanism, in which energy is transferred to the waves by shear-stress fluctuations in phase with the surface elevation (cf. Lamb 1932, Art. 242 and Art. 350).

The Jeffreys–Miles theory is essentially linear with respect to the wave amplitude. Other linear models include those of Townsend (1972), Brooke Benjamin (1959), Knight (1977), Al-Zanaidi and Hui (1984),

Corresponding author address: Dr. Alastair D. Jenkins, Bergen Scientific Centre, IBM, Thormøhlensgate 55, N-5008 Bergen, Norway.

Jacobs (1987), Sajjadi (1988), and Croft and Sajjadi (1990). Numerous laboratory experiments and field studies have been conducted in order to quantify the wave-induced pressure fluctuations, airflows, and wind-to-wave energy flux.

Returning to the Jeffreys–Miles theory, let us consider a single sinusoidal wave component with real amplitude $\tilde{\zeta}_0$, angular frequency ω, and wavenumber k, propagating along the positive x direction, so that the sea surface displacement ζ is approximated by the real part of $\tilde{\zeta}_0 \exp[i(kx - \omega t)]$, where t is time. The theory predicts that an oscillatory stress field given by $\mathrm{Re}\tilde{\sigma}_{jl}(0) \exp[i(kx - \omega t)]$, applied just above the surface, will transfer energy into the wave field at the rate of approximately

$$\rho_w g S_{\mathrm{in}} = \tfrac{1}{2}\omega\tilde{\zeta}_0[-\mathrm{Im}\tilde{\sigma}_{33}(0) + \mathrm{Re}\tilde{\sigma}_{31}(0)] \quad (1.1)$$

per unit area and time. The approximation is valid to $O(\epsilon^2)$, where $\epsilon = k\tilde{\zeta}_0$ is the wave slope. The water density is ρ_w, and g is the acceleration due to gravity. The "Re" and "Im" give real and imaginary parts, respectively, of complex expressions. The indices j and l of the stress tensor are labeled 1, 2, and 3 for the x, y, and z directions, respectively. The total stress $\sigma_{jl} = \sigma_{lj}$, shear stress τ_{jl}, and pressure p are related by the following equations:

$$p = -\frac{1}{3}\sigma_{ll}, \quad (1.2)$$

$$\sigma_{jl} = -p\delta_{jl} + \tau_{jl}, \quad (1.3)$$

where repeated indices are summed from 1 to 3 and $\delta_{jl} = 1$ if $j = l$, 0 otherwise. The tilde are used to represent complex amplitudes of wave-correlated fluctuations and the argument (0) represents the value at the sea surface.

The total wave energy per unit area is, to $O(\epsilon^2)$, $\frac{1}{2}\rho_w g\tilde{\zeta}_0^2$. From (1.1)–(1.3) we have

$$S_{\mathrm{in}} = \frac{\omega[\mathrm{Im}\tilde{p}(0) - \mathrm{Im}\tilde{\tau}_{33}(0) + \mathrm{Re}\tilde{\tau}_{31}(0)]}{\rho_w g\tilde{\zeta}_0} F, \quad (1.4)$$

where $F = \frac{1}{2}\tilde{\zeta}_0^2$ is the wave "energy"—by convention equal to the total wave energy per unit area divided by $\rho_w g$, and S_{in} is the rate at which this energy is supplied to the waves.

The waves can be thought of as having a certain amount of momentum per unit area [for a discussion of the concept of wave momentum, see McIntyre (1981)]. It is, to $O(\epsilon^2)$, equal to $\Pi = \rho_w g F/c_{\mathrm{p}}$, where $c_{\mathrm{p}} = \omega/k$ is the phase speed of the waves. Thus, the rate at which momentum is supplied to the waves from the atmosphere is

$$\Pi_{\mathrm{in}} = \tfrac{1}{2}k\tilde{\zeta}_0[\mathrm{Im}\tilde{p}(0) - \mathrm{Im}\tilde{\tau}_{33}(0) + \mathrm{Re}\tilde{\tau}_{31}(0)]. \quad (1.5)$$

For the case of a random sea state, we can represent the sea surface approximately by a discrete Fourier sum (e.g., Hasselmann 1974),

$$\begin{bmatrix} \zeta(x, y, t) \\ \sigma_{jl}(x, y, \zeta, t) \end{bmatrix} = \mathrm{Re}\sum_{\mathbf{k}} \begin{bmatrix} \tilde{\zeta}_{\mathbf{k}0} \\ \tilde{\sigma}_{jl,\mathbf{k}}(0) \end{bmatrix} \exp[i(\mathbf{k}\cdot\mathbf{x} - \omega t)]. \quad (1.6)$$

Here, $\mathbf{k} = (k_1, k_2)$ is the wavenumber vector and $\mathbf{x} = (x, y)$ is the horizontal position. The dependence of ω upon $\mathbf{k}$ is given by the appropriate dispersion relation, and the $\tilde{\zeta}_{\mathbf{k}0}$ are complex. Equations (1.4) and (1.5) become

$$S_{\mathrm{in},\mathbf{k}} = \frac{1}{\rho_w g}\omega(\mathbf{k})\left[\mathrm{Im}\frac{\tilde{p}_{\mathbf{k}}(0) - \tilde{\tau}_{33,\mathbf{k}}(0)}{\tilde{\zeta}_{k0}} + \mathrm{Re}\frac{\tilde{\tau}_{31,\mathbf{k}}(0)k_1 + \tilde{\tau}_{32,\mathbf{k}}(0)k_2}{k\tilde{\zeta}_{\mathbf{k}0}}\right]F_{\mathbf{k}}, \quad (1.7)$$

$$\boldsymbol{\Pi}_{\mathrm{in}} = \rho_w g\sum_{\mathbf{k}}\frac{\mathbf{k}}{\omega}S_{\mathrm{in},\mathbf{k}}, \quad (1.8)$$

where $F_{\mathbf{k}} = \frac{1}{2}|\tilde{\zeta}_{\mathbf{k}0}|^2$ is the wave "energy" contribution at wavenumber $\mathbf{k}$, $S_{\mathrm{in},\mathbf{k}}$ is the rate at which energy is supplied to this wavenumber component, $\tilde{p}_{\mathbf{k}}$ and $\tilde{\tau}_{jl,\mathbf{k}}$ are the Fourier components of the pressure and shear-stress fluctuations at wavenumber $\mathbf{k}$, $k = |\mathbf{k}|$, and $\boldsymbol{\Pi}_{\mathrm{in}}$ is the momentum input vector.

If the wave field is specified using a directional energy spectrum $F(f, \theta)$, where $f = \omega/(2\pi)$ and θ is the wave direction, we have

$$F \equiv \sum_{\mathbf{k}} F_{\mathbf{k}} = \int_0^\infty df\int_0^{2\pi} d\theta F(f, \theta), \quad (1.9)$$

and

$$\boldsymbol{\Pi}_{\mathrm{in}} = \rho_w g\iint df d\theta\frac{\mathbf{k}(f, \theta)}{2\pi f}S_{\mathrm{in}}(f, \theta), \quad (1.10)$$

where $S_{\mathrm{in}}(f, \theta)$ bears the same relation to $S_{\mathrm{in},\mathbf{k}}$ as $F(f, \theta)$ does to $F_{\mathbf{k}}$.

Several simple forms for $S_{\mathrm{in}}(f, \theta)$ have some experimental support. Snyder et al. (1981) found that

$$S_{\mathrm{in}}(f, \theta) = \alpha_S\frac{\rho}{\rho_w}\left[\frac{U(5\ \mathrm{m})}{c_{\mathrm{p}}}\cos(\theta - \theta_w) - 1\right] \times 2\pi f F(f, \theta), \quad 0.2 \leqslant \alpha_S \leqslant 0.3, \quad (1.11)$$

for $1 \leqslant U(5\ \mathrm{m})/c_{\mathrm{p}} \leqslant 3$, where $U(5\ \mathrm{m})$ is the wind speed at 5 m above the sea surface, θ_w is the wind direction, and ρ is the air density. Other forms include

$$S_{\mathrm{in}}(f) \propto \left[\left(\frac{8}{3\pi}\right)\frac{U(10\ \mathrm{m})}{c_{\mathrm{p}}} - 1\right]^2 fF(f)$$

(Hsiao and Shemdin 1983) and $S_{\mathrm{in}}(f) \propto (U_*/$

$c_p)^2 fF(f)$, where U_* is the wind friction velocity (Plant 1982; Mitsuyasu and Honda 1982).

The above expressions lead to results that are obviously invalid if they are used with certain wave spectra. In particular, for high-frequency deep-water gravity waves, with $\omega^2 = gk$, the Snyder et al. relation gives $S_{in}(f) \propto f^2 F(f)$, and the other relations give $S_{in}(f) \propto f^3 F(f)$. From (1.10) we see that if the high-frequency tail of the wave spectrum is of the form $F(f) \propto f^{-\beta}$, the total rate of momentum transfer from the atmosphere to the waves becomes unbounded if $\beta \leq 4$ for the Snyder et al. relation, and if $\beta \leq 5$ for the other relations. This unboundedness should not happen, since the total momentum flux from the atmosphere to the ocean should be equal to the (finite) wind stress, $\tau_w \equiv \rho U_*^2$, no matter how "pathological" the shape of the sea surface is.

Although $\Pi_{in} \equiv |\mathbf{\Pi}_{in}|$ can be made finite, for example, by setting $F(f) = 0$ above some cutoff frequency, it is more satisfactory on physical grounds to formulate $S_{in}(f, \theta)$ in such a way that the whole of $\mathbf{\Pi}_{in}$ can come from the wind stress; that is, $\Pi_{in} \leq \max[0, \tau_w \cos(\theta_{\Pi_{in}} - \theta_w)]$ where $\theta_{\Pi_{in}}$ is the direction of $\mathbf{\Pi}_{in}$, irrespective of the form of the wave spectrum. Unlike (1.11) and the other simple forms, such a formulation cannot be linear in $F(f, \theta)$, since we can just multiply a given functional form of $F(f, \theta)$ by a constant factor to make Π_{in} exceed the above limit. It is possible to eliminate this problem by using a nonlinear theory or numerical model, which was done by Miles (1965), Lee (1972), Gent and Taylor (1976), Taylor and Gent (1978), Caponi et al. (1982), Chalikov (1978, 1986a,b), Makin (1980, 1982, 1987), and Makin and Panchenko (1986). Chalikov, Makin and Panchenko employed a turbulence closure scheme over a time-varying sea surface that was generated from a large number of Fourier components and is thus computationally expensive.

An approach that in principle requires much less computation is the use of the quasi-linear approximation, in which the mean $O(\epsilon^2)$ properties of the airflow above the waves are taken into account and are allowed to influence the ratios $\tilde{p}_k(0)/\tilde{\zeta}_{k0}$ and $\tilde{\tau}_{jl,k}(0)/\tilde{\zeta}_{k0}$ in (1.7), but where we ignore higher-order perturbations and any $O(\epsilon^2)$ quantities that fluctuate on time scales of order ω^{-1} or horizontal spatial scales of order k^{-1}. This neglect of fluctuating $O(\epsilon^2)$ quantities can be justified by observing that there is no resonant interaction at this order between different free-surface gravity wave Fourier components (Phillips 1960; Hasselmann 1962).

The quasi-linear approximation was implemented by Fabrikant (1976) and Janssen (1982, 1989) using the Eulerian hydrodynamic equations in a Cartesian coordinate system for the airflow above the waves. Janssen et al. (1989) applied the technique to determine the effect of waves on the atmospheric boundary layer, using a spectral wave model to calculate the wave field. The use of a Cartesian coordinate system has the disadvantage that one has to deal with conditions at an irregular moving boundary, and the interpretation of calculated mean velocity fields, etc., is difficult at levels below the wave crests. Since we may expect a boundary layer to form near the sea surface, in which the velocity field can have large vertical gradients, this may be a significant problem. Miles, Fabrikant, and Janssen also assumed that the oscillatory part of the flow field induced by the waves could be regarded as unaffected by viscosity or turbulence.

In this paper the quasi-linear approximation is implemented using a time-dependent curvilinear coordinate system, in which one of the coordinate surfaces is made to coincide with the water surface. Curvilinear coordinates have been used for airflow over waves by many authors (e.g., Miles 1959, 1962; Brooke Benjamin 1959; Lee 1972; Gent and Taylor 1976; Knight 1977; Makin 1980, 1982, 1987; Hsu et al. 1981; Caponi et al. 1982; Al-Zanaidi and Hui 1984; Sajjadi 1988; Croft and Sajjadi 1990). To the author's knowledge, however, the curvilinear coordinate approach has not been applied previously in combination with the quasi-linear approximation for airflow over water waves. Turbulent stresses are parameterized by using an eddy viscosity that acts upon the oscillatory part as well as the mean part of the flow field.

2. Mathematical formulation

a. Introduction

In a Cartesian coordinate system, $(x, y, z) \equiv (x_1, x_2, x_3) \equiv \mathbf{x}$, we assume that the air velocity field, $\mathbf{u} \equiv (u_1, u_2, u_3) \equiv (u, v, w)$ obeys the following equations of incompressible fluid flow:

$$\rho\left(\frac{\partial u_j}{\partial t} + u_l \frac{\partial u_j}{\partial x_l} + \frac{\partial \Phi}{\partial x_j}\right) - \frac{\partial \sigma_{jl}}{\partial x_l} = 0, \tag{2.1}$$

$$\frac{\partial \rho}{\partial t} + \frac{\partial}{\partial x_l}(\rho u_l) = \rho \frac{\partial u_l}{\partial x_l} = 0. \tag{2.2}$$

The indices in the Roman alphabet (j and l) range from 1 to 3, and the usual summation convention applies for repeated indices. Internal forces (including the Reynolds stresses of turbulent motion) are represented by the stress components $\sigma_{jl} = -p\delta_{jl} + \tau_{jl}$. The force of gravity is determined by the gravitational potential, $\Phi = gx_3$, and t is time. The air density ρ is constant.

The equations can be written in conservation-law form (e.g., Anderson et al. 1968; Eiseman and Stone 1980; Navon 1983; Majda 1984):

$$\frac{\partial \phi}{\partial t} + \frac{\partial F_l}{\partial x_l} = 0. \tag{2.3}$$

Here, $\phi dx_1 dx_2 dx_3$ is the amount of a conserved quantity (mass or one of the Cartesian components of mo-

mentum) contained in an infinitesimal rectangular parallelepiped with sides dx_1, dx_2, and dx_3 parallel to the corresponding coordinate axes, and $F_l dx_j dx_m (l, j,$ and m being different from each other) is the amount of the conserved quantity flowing per unit time interval in the positive x_l direction through an infinitesimal rectangle with sides dx_j and dx_m. (This flux F_l should not be confused with the wave energy spectrum F_k.)

In (2.1), $\phi = \rho u_j$, and $F_l = \rho(u_j u_l + \Phi\delta_{jl}) - \sigma_{jl}$ ($j = 1, 2, 3$). In (2.2), $\phi = \rho =$ const, and $F_l = \rho u_l$.

b. Transformation to a curvilinear coordinate system

An equation of the form (2.3) in Cartesian coordinates has a direct equivalent in a curvilinear coordinate system, $(y_1, y_2, y_3) \equiv (a, b, c) \equiv \mathbf{y}$, provided that the coordinate transformation mapping, $\mathbf{x}(\mathbf{y}, t)$, is invertible and sufficiently differentiable:

$$\frac{\partial \psi}{\partial t} + \frac{\partial G_l}{\partial y_l} = 0. \tag{2.4}$$

The quantity $\psi dy_1 dy_2 dy_3$ now represents the amount of the same conserved quantity as in (2.3) contained in an infinitesimal parallelepiped with sides dy_1, dy_2, and dy_3 parallel to the *local* $\mathbf{y}$-coordinate directions. In this case, the parallelepiped will, in general, not be rectangular and will be moving with respect to the Cartesian coordinate system $\mathbf{x}$. The amount of the conserved quantity that flows—with respect to the $\mathbf{y}$-coordinate system—in the direction of increasing y_l through the infinitesimal moving parallelogram with sides dy_j and dy_m parallel to the local y_j and y_m coordinate directions (l, j, and m all being unequal), is given by $G_l dy_j dy_m$.

Equation (2.4) was derived from (2.3) by Anderson et al. (1968), Vinokur (1974), and Eiseman and Stone (1980), using general tensor analysis. A version of the derivation is repeated below, using a somewhat different notation than is used by the above authors—the notation resembles that of Andrews and McIntyre (1978).

We use four-dimensional coordinate systems, identifying time with the fourth coordinate direction in both the $\mathbf{x}$ and $\mathbf{y}$ systems. If we adopt the convention that Greek indices range from 1 to 4, and repeated Greek indices are summed correspondingly, (2.3) becomes

$$\frac{\partial F_\mu}{\partial x_\mu} = 0, \tag{2.5}$$

where $F_4 = \phi$. Transforming to the $\mathbf{y}$-coordinate system, we have

$$\frac{\partial F_\mu}{\partial y_\lambda}\frac{\partial y_\lambda}{\partial x_\mu} = \frac{\partial F_\mu}{\partial y_\lambda}\frac{K_{\mu\lambda}^{(4)}}{J^{(4)}} = 0, \tag{2.6}$$

where $J^{(4)}$ is the determinant of the 4×4 Jacobian matrix $[\partial x_\mu / \partial y_\lambda]$, and the $K_{\mu\lambda}^{(4)}$ are its cofactors.

If we make the substitution $G_\mu = K_{\lambda\mu}^{(4)} F_\lambda$ and use the relation $\partial K_{\lambda\mu}^{(4)}/\partial y_\mu = 0$ [obtained by extending the corresponding result in Appendix A of Andrews and McIntyre (1978) to four dimensions], we end up with $\partial G_\mu / \partial y_\mu = 0$, so that in three dimensions, (2.4) is satisfied with $\psi = G_4$.

In terms of the determinant J and cofactors K_{jl} of the 3×3 Jacobian matrix $[\partial x_j / \partial y_l]$, $J^{(4)}$ and $K_{\lambda\mu}^{(4)}$ can be expressed as follows:

$$\begin{aligned} J^{(4)} &= J, \\ K_{jl}^{(4)} &= K_{jl}, \\ K_{j4}^{(4)} &= 0, \\ K_{4l}^{(4)} &= -K_{ml}\frac{\partial x_m}{\partial t}, \\ K_{44}^{(4)} &= J. \end{aligned} \tag{2.7}$$

Hence,

$$\begin{aligned} G_j &= K_{lj} F_l - K_{lj}\phi \frac{\partial x_l}{\partial t} \\ \psi = G_4 &= J\phi. \end{aligned} \tag{2.8}$$

We can now write the momentum equation (2.1) as

$$\frac{\partial P_j}{\partial t} - \frac{\partial T_{jl}}{\partial y_l} = 0, \tag{2.9}$$

where $P_j = \rho J u_j$ and

$$T_{jl} = \left(\rho u_j \frac{\partial x_m}{\partial t} - \rho u_j u_m + \sigma_{jm}\right) K_{ml} - \rho \Phi K_{jl}. \tag{2.10}$$

The continuity equation (2.2) becomes

$$\frac{\partial}{\partial t}(\rho J) + \frac{\partial}{\partial y_l}\left[K_{ml}\rho\left(u_m - \frac{\partial x_m}{\partial t}\right)\right] = \rho K_{ml}\frac{\partial u_m}{\partial y_l} = 0. \tag{2.11}$$

Note that, while the partial derivatives are now with respect to the curvilinear coordinates, y_j, the components of the forces, velocities, and momenta are still in the directions of the Cartesian coordinate axes, x_j (cf. Shyy and Vu 1991).

The quantities P_j can be thought of as representing the concentration of x_j momentum in $\mathbf{y}$ space, and $-T_{jl}$ represents the flux in the positive y_l direction of x_j momentum across surfaces of constant y_l.

c. Mean and fluctuating parts

We now express all dependent variables, including the Cartesian coordinates $\mathbf{x}(\mathbf{y}, t)$, as sums of mean and fluctuating parts: $q(\mathbf{y}, t) = \bar{q} + q'$, where $\overline{(\bar{q})} = \bar{q}$, $\overline{q'} = 0$, $\overline{\partial q/\partial y_j} = \partial \bar{q}/\partial y_j$ and $\overline{\partial q(\mathbf{y}, t)/\partial t} = \partial \bar{q}(\mathbf{y}, t)/\partial t$. The averaging operator can, for example, be an ensemble average, or an average over some suitably long time (keeping $\mathbf{y}$ constant) or some suitably large

region in $\mathbf{y}$ space. Such an average corresponds to an Eulerian mean if $\mathbf{x} = \mathbf{y}$, and it corresponds to a Lagrangian mean if $\partial\mathbf{x}/\partial t = \mathbf{u}$. The generalized Lagrangian mean of Andrews and McIntyre (1978) is reproduced if $\bar{\mathbf{x}} = \mathbf{y}$ and $\partial\mathbf{x}/\partial t + \overline{u_l}\partial\mathbf{x}/\partial y_l = \mathbf{u}$.

From (2.9) we obtain $\partial\bar{P}_j/\partial t - \partial\bar{T}_{jl}/\partial y_l = 0$ and $\partial P_j'/\partial t - \partial T_{jl}'/\partial y_l = 0$, where the mean and fluctuating parts of P_j and T_{jl} can be evaluated in a relatively straightforward manner. The continuity equation (2.11) can also be decomposed into mean and fluctuating parts.

d. Coordinate system and wave field

We choose the curvilinear coordinate system such that $\mathbf{x} = \mathbf{y} + \boldsymbol{\xi}$, $\boldsymbol{\xi} \equiv (\xi_1, \xi_2, \xi_3) \equiv (\xi, \eta, \zeta)$, with

$$\begin{bmatrix} \xi \\ \eta \\ \zeta \end{bmatrix} = \mathrm{Re} \sum_{\mathbf{k}} \begin{bmatrix} i\cos\theta \\ i\sin\theta \\ 1 \end{bmatrix} \tilde{\zeta}_{\mathbf{k}}(c) \exp[i(\mathbf{k}\cdot\mathbf{y} - \omega t)], \tag{2.12}$$

where $\mathbf{k} = (k\cos\theta, k\sin\theta, 0)$, $\omega = (gk)^{1/2}[1 + \mathrm{O}(\epsilon^2)]$, and $\tilde{\zeta}_{\mathbf{k}}(c) = \tilde{\zeta}_{\mathbf{k}0}e^{-kc}$. The sea surface, $c = 0$, can be regarded as a Fourier sum of deep-water gravity waves of a form similar to those described by Gerstner (1804), and we have $\bar{\mathbf{x}} = \mathbf{y}$, $\bar{\boldsymbol{\xi}} = 0$. As is the case with real ocean waves, the crests of the waves are sharper than the troughs. If waves of finite amplitude are generated from an initial state with $\boldsymbol{\xi} = 0$, mass conservation requires a nonzero $\mathrm{O}(\epsilon^2)$ mean vertical displacement $\bar{\zeta}_0 = (1/2)\Sigma_{\mathbf{k}} k|\tilde{\zeta}_{\mathbf{k}0}|^2$ (Pierson 1961; Chang 1969). We can remove this displacement by a vertical translation of the coordinates. If more than one Fourier component is present, the true $\mathrm{O}(\epsilon^2)$ form of the surface will contain "bound waves" with $k \neq (\omega^2/g)[1 + \mathrm{O}(\epsilon^2)] \neq 0$, created by second-order interactions; but we shall neglect those, consistent with the assumption of the quasilinear approximation.

We now just consider disturbances in the xz plane, for which $J = 1 + \xi_a + \zeta_c + \xi_a\zeta_c - \xi_c\zeta_a$, $K_{11} = 1 + \zeta_c$, $K_{13} = -\zeta_a$, $K_{31} = -\xi_c$, and $K_{33} = 1 + \xi_a$, where we use the notation $(\cdot)_a$ for $\partial(\cdot)/\partial y_1$, etc. We assume that $u_1 = u = U(c) + u'(a, c, t)$, $u_2 = 0$, $u_3 = w = \bar{w}(c) + w'(a, c, t)$, $p = \bar{p}(c) + p'(a, c, t)$, $\tau_{11} = -\tau_{33} = \bar{\tau}_{11}(c) + \tau_{11}'(a, c, t) = -\bar{\tau}_{33}(c) - \tau_{33}'(a, c, t)$, and $\tau_{13} = \tau_{31} = \bar{\tau}_{13}(c) + \tau_{13}'(a, c, t) = \bar{\tau}_{31}(c) + \tau_{31}'(a, c, t)$. The mean quantities (including mean products of any two fluctuating quantities) are assumed to depend only upon the vertical coordinate, and the shear-stress tensor is assumed to be symmetric.

In reality, the mean quantities and the wave Fourier components $\tilde{\zeta}_{\mathbf{k}0}$ will vary with the horizontal coordinates and time (necessarily so if we have wave growth due to wind-induced stress fluctuations at the sea surface). I assume, however, that such variations are so slow that the changes that they induce in the following equations are negligible.

We regard the mean quantities U, $\bar{p}$, and $\bar{\tau}_{13} = \bar{\tau}_{31}$ as being $\mathrm{O}(1)$, the other mean quantities, $\bar{w}$ and $\bar{\tau}_{11} = -\bar{\tau}_{33}$, as being $\mathrm{O}(\epsilon^2)$, and the fluctuating quantities as $\mathrm{O}(\epsilon)$. The mean momentum and continuity equations take the form $\partial\bar{G}_3/\partial y_3 = 0$, so that $\bar{G}_3 = \text{const}$, independent of c. Thus, to $\mathrm{O}(\epsilon^2)$,

$$\bar{\tau}_{13} - \rho U\bar{w} + \overline{p'\zeta_a} - \overline{\tau_{11}'\zeta_a} + \overline{\tau_{13}'\xi_a} + \rho[g\overline{\zeta\zeta_a} + \overline{u'\zeta_t} - \overline{u'w'} + U(\overline{\xi_a\zeta_t} - \overline{\xi_t\zeta_a} + 2\overline{u'\zeta_a} - \overline{w'\xi_a})] = \tau_w, \tag{2.13}$$

$$\bar{p} - \bar{\tau}_{33} = -\rho gc + \rho g\overline{\zeta\zeta_a} - \overline{p'\xi_a} + \overline{\tau_{33}'\xi_a} - \overline{\tau_{31}'\zeta_a} + \rho\overline{w'\zeta_t} + \rho U\overline{w'\zeta_a} - \rho\overline{w'w'}, \tag{2.14}$$

$$\bar{w} = \overline{u'\zeta_a} - \overline{w'\xi_a} + \overline{\xi_a\zeta_t} - \overline{\xi_t\zeta_a}. \tag{2.15}$$

The value of the integration constant in (2.13) is determined by the condition $\bar{\tau}_{13} \to \tau_w$ as $c \to \infty$; in (2.14) it is chosen arbitrarily, and in (2.15) it is determined by ($\bar{w} \to 0$, $c \to \infty$). Combining (2.13) and (2.15), we obtain

$$\bar{\tau}_{13} + \overline{p'\zeta_a} - \overline{\tau_{11}'\zeta_a} + \overline{\tau_{13}'\xi_a} + \rho(\overline{u'\zeta_t} - \overline{u'w'} + U\overline{u'\zeta_a} + g\overline{\zeta\zeta_a}) = \tau_w. \tag{2.16}$$

The last term on the left-hand side of (2.16), $\rho g\overline{\zeta\zeta_a}$, is equal to zero if the coordinate displacement $\boldsymbol{\xi}$ is of the form $\mathrm{Re}\,\Sigma_{\mathbf{k}}\tilde{\boldsymbol{\xi}}_{\mathbf{k}}(c)\exp[i(\mathbf{k}\cdot\mathbf{y} - \omega t)]$; that is, if it has traveling-wave behavior.

We obtain a set of $\mathrm{O}(\epsilon)$ equations for the Fourier components $\tilde{q}_{\mathbf{k}}$ of the fluctuating quantities q', from (2.9)–(2.12). We neglect the $\mathrm{O}(\epsilon^2)$ quantities $\bar{w}$ and $\bar{\tau}_{11}$, and the $\mathrm{O}(\epsilon^2)$ difference between $\bar{p}$ and $-\rho gc$. Using nondimensional quantities, $\check{c} = kc$, $\check{\omega} = \omega/(gk)^{1/2}$, $\check{U} = U/(g/k)^{1/2}$, $\check{\bar{\tau}} = k\bar{\tau}_{13}/(\rho g)$, $\check{\zeta}_{\mathbf{k}} = \tilde{\zeta}_{\mathbf{k}}/\tilde{\zeta}_{\mathbf{k}0}$, $\check{u}_{\mathbf{k}} = \tilde{u}_{\mathbf{k}}/[(gk)^{1/2}\tilde{\zeta}_{\mathbf{k}0}]$, $\check{w}_{\mathbf{k}} = \tilde{w}_{\mathbf{k}}/[(gk)^{1/2}\tilde{\zeta}_{\mathbf{k}0}]$, $\check{p}_{\mathbf{k}} = \tilde{p}_{\mathbf{k}}/(\rho g\tilde{\zeta}_{\mathbf{k}0})$, $\check{\tau}_{11,\mathbf{k}} = \tilde{\tau}_{11,\mathbf{k}}/(\rho g\tilde{\zeta}_{\mathbf{k}0})$, and $\check{\tau}_{13,\mathbf{k}} = \tilde{\tau}_{13,\mathbf{k}}/(\rho g\tilde{\zeta}_{\mathbf{k}0})$, we obtain:

$$\begin{bmatrix} i(\check{U} - \check{\omega}) & \check{U}_{\check{c}} & i & -i & -\partial/\partial\check{c} \\ 0 & i(\check{U} - \check{\omega}) & \partial/\partial\check{c} & \partial/\partial\check{c} & -i \\ i & \partial/\partial\check{c} & 0 & 0 & 0 \end{bmatrix} \times \begin{bmatrix} \check{u}_{\mathbf{k}} \\ \check{w}_{\mathbf{k}} \\ \check{p}_{\mathbf{k}} \\ \check{\tau}_{11,\mathbf{k}} \\ \check{\tau}_{13,\mathbf{k}} \end{bmatrix} = \begin{bmatrix} i(\check{U}\check{U}_{\check{c}} - \check{\omega}\check{U}_{\check{c}} - 1) - \check{\bar{\tau}}_{\check{c}} \\ 1 - i\check{\bar{\tau}}_{\check{c}} \\ i\check{U}_{\check{c}} \end{bmatrix} \check{\zeta}_{\mathbf{k}}. \tag{2.17}$$

The mean product terms in (2.13)–(2.16) can be obtained from the Fourier components by the following relation, for two variables q and r:

$$\overline{q'r'} = \frac{1}{2}\mathrm{Re}\sum_{\mathbf{k}} \tilde{q}_{\mathbf{k}}^*\tilde{r}_{\mathbf{k}}, \tag{2.18}$$

where $(\cdot)^*$ denotes the complex conjugate.

e. Turbulence closure

A complete set of equations can now be obtained from (2.16) and (2.17) if we specify how to determine $\bar{\tau}_{13}$ and $\tilde{\tau}_{jl,\mathbf{k}}$. I do this by making use of a simple "turbulence closure" hypothesis.

The velocity components u_j are assumed to consist only of mean values and wave-associated fluctuations. Those fluctuations due to turbulent motions are averaged out, and their effect on the mean and wave-associated flow is incorporated in the stress σ_{jl}, using a simple "eddy viscosity" concept. I assume that the mean shear stress is proportional to the O(1) part of the symmetric velocity gradient

$$\frac{\partial u_j}{\partial x_l} + \frac{\partial u_l}{\partial x_j} = \frac{1}{J}\left(K_{lm}\frac{\partial u_j}{\partial y_m} + K_{jm}\frac{\partial u_l}{\partial y_m}\right), \quad (2.19)$$

which is traceless by (2.2), and that the fluctuating shear stress is proportional to the O(ϵ) part. The constant of proportionality is called the "total viscosity" ν, which I assume to be a function of c alone. It includes the Newtonian molecular viscosity as well as the turbulent eddy viscosity.

We then have

$$\bar{\tau}_{13} = \rho\nu(c)U_c, \quad (2.20)$$

$$\tau'_{11} = 2\rho\nu(c)(u'_a - U_c\zeta_a) \quad (2.21)$$

and

$$\tau'_{13} = \rho\nu(c)(u'_c + w'_a - U_c\zeta_c), \quad (2.22)$$

from which

$$\begin{bmatrix} -2i\check{\nu} & 0 & 0 & 1 & 0 \\ -\check{\nu}\partial/\partial\check{c} & -i\check{\nu} & 0 & 0 & 1 \end{bmatrix} \begin{bmatrix} \check{u}_{\mathbf{k}} \\ \check{w}_{\mathbf{k}} \\ \check{\tau}_{11,\mathbf{k}} \\ \check{\tau}_{13,\mathbf{k}} \end{bmatrix} = \begin{bmatrix} -2i\check{\nu}\check{U}_{\check{c}} \\ \check{\nu}\check{U}_{\check{c}} \end{bmatrix} \check{\zeta}_{\mathbf{k}}, \quad (2.23)$$

with $\check{\nu} = (\omega k/g)\nu$. Note that if $\check{\nu}$ is constant and $\check{\bar{\tau}}_{\check{c}} = 0$, (2.17, 2.20, 2.23) can be reduced to the Orr–Sommerfeld equation (dropping the $\mathbf{k}$ subscripts):

$$(\check{U} - \check{\omega})\check{w}_{\check{c}\check{c}} - [(\check{U} - \check{\omega}) + \check{U}_{\check{c}\check{c}}]\check{w} = -i\check{\nu}(\check{w}_{\check{c}\check{c}\check{c}\check{c}} - 2\check{w}_{\check{c}\check{c}} + \check{w}). \quad (2.24)$$

If $\check{\nu} = 0$, the right-hand side of (2.24) vanishes, and we obtain the Rayleigh equation, on which the linear computations of Miles (1957) and Conte and Miles (1959) and the quasi-linear computations of Janssen (1989) are based. In this paper the full set of primitive equations [(2.17), (2.23)] will be used, so that we do not have to resort to numerical differentiation when computing the mean quadratic terms in (2.16).

With a nonzero total viscosity, the singularity that appears in the solution to the Rayleigh equation at the critical height, where $U = c_p$, disappears, being effectively spread out over a finite layer thickness. Were we to use the generalized Lagrangian mean formulation of Andrews and McIntyre (1978), there would be a singularity in the coordinate system at the critical height, which would not disappear (Craik 1982).

In the following sections, the following formulation for the total viscosity is used:

$$\nu = \nu_m + \kappa(c + z_0)(\bar{\tau}_{13}/\rho)^{1/2}, \quad (2.25)$$

where ν_m is the Newtonian molecular viscosity, taken to be 0.14×10^{-4} m^2 s^{-1}; $\kappa = 0.4$ is von Kármán's constant; and z_0 is the roughness length. If we ignore ν_m and combine (2.25) with (2.20), in the absence of waves we obtain Prandtl's (1925) mixing length formula $\bar{\tau}_{13} = \rho l^2|\partial U/\partial z|(\partial U/\partial z)$, with $l = \kappa(z + z_0)$. For the roughness length I use the Charnock (1955) relation

$$z_0 = \alpha\tau_w/(\rho g) \quad (2.26)$$

with $\alpha = 0.0144$ (cf. Janssen 1989).

f. Boundary conditions

At the air–water interface $c = 0$, the velocity $\mathbf{u}$ and all the stress components σ_{jl} are continuous. We can use these interfacial conditions to match the airflow with the water flow in the waves.

To O(ϵ), the surface velocity in deep-water gravity waves without friction is given by $\mathbf{u}' = \partial\boldsymbol{\xi}/\partial t$; that is,

$$\begin{bmatrix} u' \\ v' \\ w' \end{bmatrix} = \mathrm{Re}\sum_{\mathbf{k}} \begin{bmatrix} \omega\cos\theta \\ \omega\sin\theta \\ -i\omega \end{bmatrix} \tilde{\zeta}_{\mathbf{k}0} \exp[i(\mathbf{k}\cdot\mathbf{y} - \omega t)], \quad c = 0. \quad (2.27)$$

In the nondimensional notation of (2.17), we thus have

$$\check{u}_{\mathbf{k}} = \check{\omega}, \quad \check{w}_{\mathbf{k}} = -i\check{\omega}, \quad c = 0. \quad (2.28)$$

There is a correction to the O(ϵ) surface velocity if the water viscosity ν_w is nonzero (Longuet-Higgins 1953), of order $(2\nu_w k^2/\omega)^{1/2}|\mathbf{u}'|$; but this can normally be neglected, even if we substitute an eddy viscosity for ν_w to take account of turbulent motions.

Since to O(ϵ) the coordinate points at $c = 0$ follow the movement of the water particles, to O(ϵ^2) the mean velocity $\bar{\mathbf{u}}$ is equal to the mass transport velocity or Lagrangian mean current—the mean velocity obtained when we follow the water particle paths (Pollard 1973; Andrews and McIntyre 1978). This surface current will have a complicated nonstationary dependence on the stress conditions at the surface, the rotation of the earth, and wavelike and dissipative processes within the water column (e.g., Stokes 1847; Longuet-Higgins 1953; Liu and Davis 1977; Weber 1983, 1990; Jenkins 1987). For simplicity, we use the value chosen by Janssen [1989, Eq. (19)],

$$\bar{\mathbf{u}} = 0, \quad c = 0, \quad (2.29)$$

together with the dispersion relation

$$\omega^2 = gk; \quad \text{i.e.} \quad \breve{\omega} = 1. \tag{2.30}$$

These conditions are satisfied by finite-amplitude Gerstner waves (Gerstner 1804). (We assume that the dispersion relation is unaffected by the airflow over the waves.)

At the top of the domain we specify a fixed applied wind stress

$$\bar{\tau}_{13} \to \tau_w, \quad c \to \infty \tag{2.31}$$

and zero fluctuating shear stress

$$\check{\tau}_{11,\mathbf{k}} \to 0, \quad \check{\tau}_{13,\mathbf{k}} \to 0, \quad c \to \infty. \tag{2.32}$$

g. *Energy and momentum flux*

A conservation-law equation for energy can be derived from (2.1) by multiplying by u_j, summing over j, and using (2.2) where necessary. We obtain

$$\frac{\partial E}{\partial t} + \frac{\partial \Phi_{El}}{\partial x_l} = S_E, \tag{2.33}$$

where

$$E = \tfrac{1}{2}\rho u_j u_j + \rho g x_3 \tag{2.34}$$

is the mechanical energy per unit volume,

$$\Phi_{El} = \left(\tfrac{1}{2}\rho u_j u_j + \rho g x_3\right) u_l + p u_l - \tau_{jl} u_j \tag{2.35}$$

is the flux of energy per unit area in the positive x_l direction, and

$$S_E = -\tau_{jl}\frac{\partial u_j}{\partial x_l} \tag{2.36}$$

is minus the rate of energy dissipation per unit volume. In curvilinear coordinates we thus have

$$\frac{\partial}{\partial t}(JE) + \frac{\partial \Phi^y_{El}}{\partial y_l} = JS_E, \tag{2.37}$$

where

$$\Phi^y_{El} = K_{ml}\left(\Phi_{Em} - E\frac{\partial x_m}{\partial t}\right) \tag{2.38}$$

can be considered to be the flux of energy in the positive y_l direction.

Considering motions in the x–z plane only, the mean upward energy flux across constant c surfaces is

$$\overline{\Phi^y_{E3}} = \overline{K_{13}\Phi_{E1}} - \overline{K_{13}E\frac{\partial x_{E1}}{\partial t}} + \overline{K_{33}\Phi_{E3}} - \overline{K_{33}E\frac{\partial x_3}{\partial t}}. \tag{2.39}$$

Applying the quasi-linear approximation, noting that $\bar{K}_{13} = 0$, we have to $O(\epsilon^2)$ at the sea surface:

$$\overline{\Phi^y_{E3}} = \bar{\tau}_{13}(-U - \overline{u'\xi_a} + \overline{w'\zeta_a}) + \rho g(\overline{w'\zeta} - \overline{\zeta\zeta_t}) + \overline{p'w'} - \overline{\tau'_{33}w'} - \overline{\tau'_{13}u'}, \quad c = 0. \tag{2.40}$$

Applying the sea surface boundary conditions $u' = \xi_t$, $w' = \zeta_t$, with $|\tilde{\xi}_\mathbf{k}| = |\tilde{\zeta}_\mathbf{k}|$ for all Fourier components, we obtain

$$-\overline{\Phi^y_{E3}} = +\bar{\tau}_{13}U - \overline{p'\zeta_t} + \overline{\tau'_{33}\zeta_t} + \overline{\tau'_{13}\xi_t}, \quad c = 0,$$
$$= \bar{\tau}_{13}(0)U(0) + \rho_w g \sum_\mathbf{k} S_{\text{in},\mathbf{k}}. \tag{2.41}$$

The above expression is the quasi-linear approximation to the total flux of mechanical energy from the atmosphere to the ocean. The first term (on the right-hand side of the first line) is the energy flux due to the mean flow and the purely turbulent motions. The other three terms correspond to the contributions of the three terms in (1.4) to the rate of wave energy input from the pressure and shear-stress fluctuations at the sea surface.

If we apply the same surface boundary conditions to the mean horizontal momentum equation (2.16), we obtain to $O(\epsilon^2)$,

$$\tau_w = \bar{\tau}_{13} + \overline{p'\zeta_a} - \overline{\tau'_{11}\zeta_a} + \overline{\tau'_{13}\xi_a}, \quad c = 0. \tag{2.42}$$

The momentum flux to the waves cannot, however, be calculated by adding up the last three terms in this equation—it is necessary to use the three last terms in the first line of (2.41) and the relation between wave momentum and energy input (1.8).

If we compare (2.41) with (2.42), we see that the second term (the pressure fluctuation term) gives a flux of horizontal momentum in the same direction as the energy flux. The third and fourth terms, however, give momentum fluxes in the opposite direction (e.g., upward if the energy flux is downward). In the case of the diagonal components τ'_{11} and τ'_{33} of the shear stress, the flux reversal is a consequence of their sum being zero. In the case of the off-diagonal shear-stress component τ'_{13}, it is because the a-coordinate surfaces are closer together near the wave crests than in the wave troughs, so that if τ'_{13} is positive when ζ is a maximum, the mean horizontal force exerted by τ'_{13} on the sea surface will be in the $-x$ direction. (See also section 4d of Jenkins 1987.)

h. *Numerical solution*

The system of equations [(2.16)–(2.18), (2.20), (2.23), (2.25), (2.28)–(2.32)] is solved iteratively: first, solve the mean-flow equations (2.16), (2.20), (2.25), (2.29), (2.31) with the mean product terms set to zero; then substitute the solutions for U and $\bar{\tau}_{13}$ into the oscillatory-flow equations (2.17), (2.23), (2.28), (2.30), (2.32) to obtain a first estimate of the fluctuating variables for each wavenumber; then evaluate the mean product terms in (2.16), (2.20) using (2.18) and solve the mean-flow equations again for U and

$\bar{\tau}_{13}$, and so on. If this iterative procedure becomes unstable, convergence may be attained by underrelaxation, where if Q_n is the solution for U and $\bar{\tau}_{13}$ obtained after n iterations, and Q_n^{new} is obtained by applying the original iterative procedure to Q_n, the next iterative solution, Q_{n+1}, is calculated using the formula

$$Q_{n+1} = (1 - \lambda)Q_n + \lambda Q_n^{\text{new}} \qquad (2.43)$$

with $\lambda < 1$. Convergence is also assisted by letting the wave amplitude increase gradually from zero during the computation instead of applying the full wave field during the first iteration. The equations are solved by finite differences, using a logarithmically transformed vertical coordinate, $C = \log[(c + z_0)/z_0]$.

A two-dimensional wave spectrum can be allowed for by rotating the x direction in (2.17), (2.23) to coincide with the direction of $\mathbf{k}$, and resolving the mean quantities (now vectors) $\check{\mathbf{U}}$, $\check{\bar{\tau}}$, etc., along the same direction so that they become, for example, $\hat{\mathbf{k}} \cdot \check{\mathbf{U}}$, where $\hat{\mathbf{k}}$ is the unit vector in the $\mathbf{k}$ direction. The products of Fourier coefficients in (2.18) can then be resolved appropriately along the original x and y directions before summing to obtain the mean products for (2.16) and (2.20).

3. Results

The model was first run in a linear mode and compared with Conte and Miles' (1959) numerical solution of the Rayleigh equation and with Jacobs' (1987) perturbation approximation for turbulent airflow over waves. For these two comparisons, the molecular viscosity ν_m was set to zero.

The full quasilinear model was then run with $\nu_m = 0.14 \times 10^{-4}$ m^2 s^{-1} and the results were compared with the quasilinear model results of Janssen (1989), the turbulence closure model results of Makin and Chalikov (Chalikov 1986b), and the field observations of Maat et al. (1991), Donelan (1982, 1990), and Geernaert et al. (1987).

a. Linear model

For the linear version of the present model, we perform only the first two steps of the iterative procedure: the solution of the mean-flow equations with the quadratic terms set to zero (so that $\partial\bar{\tau}_{13}/\partial c = 0$) and the subsequent solution of the equations for oscillatory flow.

Conte and Miles (1959) solved the Rayleigh equation numerically with $U = (U_*/\kappa)\log[(z + z_0)/z_0]$, and calculated $\check{p}_k(0)$ by using (in effect) the first and third rows of (2.17), with $\check{\tau}_{11,k} = \check{\tau}_{13,k} = 0$. They tabulated the real and imaginary parts of $\check{p}_k(0)/[U_*/(\kappa c_p)]^2$ as a function of $\kappa c_p/U_*$ and $gz_0\kappa^2/U_*^2$. For the comparison, I ran the linear model with a wave frequency $f = 0.2$ Hz (so $k = 0.1610$ m^{-1} and $k^{-1} = 6.210$ m), a domain of vertical extent $c_{\max} = 500$ m, and three finite-difference meshes with 100, 1000, and 10 000 points, equally spaced in terms of $C = \log[(c + z_0)/z_0]$. The mean-flow total viscosity ν_{mean} [the ν used in (2.20)] was set equal to $\kappa U_*(c + z_0)$, and the "wave" total viscosity [used in (2.23)] was reduced to a value of $\nu_{\text{wav}} = 10^{-4}\,\nu_{\text{mean}}$ in order to approximate the nonviscous behavior. The results from the 10 000-point runs were little different from those obtained with 1000 mesh points. Table 1 shows the 100-point and 1000-point results.

TABLE 1. Comparison of rates of wave energy input produced by the linear model with those produced by the model of Conte and Miles (1959). The columns headed "Pressure" show the imaginary part of the dimensionless pressure fluctuation $\check{p}_k(0)$ divided by $[U_*/(\kappa c_p)]^2$. Those headed "Total" include the contribution from shear-stress fluctuations and are, thus, equal to $\{\text{Im}[\check{p}_k(0) - \check{\tau}_{33,k}(0)] + \text{Re}\check{\tau}_{13,k}(0)\}/[U_*/(\kappa c_p)]^2$.

		Linear model					
		$\nu_{\text{wav}}/\nu_{\text{mean}} = 10^{-4}$			$\nu_{\text{wav}}/\nu_{\text{mean}} = 1$		
Conte and Miles		1000 pts		100 pts	1000 pts		100 pts
$\kappa c_p/U_*$	Pressure	Pressure	Total	Total	Pressure	Total	Total
			$gz_0\kappa^2/U_*^2 = 3 \times 10^{-3}$				
1	3.53	3.526	3.524	3.492	2.714	3.483	3.480
4	3.43	3.431	3.430	3.372	3.111	3.657	3.599
7	2.44	2.441	2.441	2.419	3.759	4.038	3.918
10	0.405	0.404	0.404	0.306	0.433	0.610	0.597
			$gz_0\kappa^2/U_*^2 = 2 \times 10^{-2}$				
1	2.75	2.753	2.753	2.749	1.764	2.453	2.454
4	2.43	2.427	2.427	2.416	3.178	3.545	3.522
7	0.677	0.677	0.676	0.671	1.015	1.150	1.143
10	2×10^{-4}	1×10^{-4}	−0.001	0.004	−0.727	−0.720	−0.711

The linear model results for $[\mathrm{Im}\check{p}_k(0)]/[U_*/\kappa c_p)]^2$ with 1000 points and $\nu_{wav}/\nu_{mean} = 10^{-4}$ show little difference from those calculated by Conte and Miles. This is encouraging since we are performing a singular perturbation: in effect, we use a fourth-order differential equation to approximate one of second order, with "no-slip" rather than "zero flow across the interface" boundary conditions at $c = 0$. I have also tabulated the total dimensionless wave energy input $\{\mathrm{Im}[\check{p}_k(0) - \check{\tau}_{33,k}(0)] + \mathrm{Re}\check{\tau}_{13,k}(0)\}/[U_*/(\kappa c_p)]^2$ for grids of 1000 and 100 points as well as the corresponding results for $\nu_{wav} = \nu_{mean}$. The differences between the 1000-point and 100-point results for $\nu_{wav} = \nu_{mean}$ are relatively small, and to save computer time a mesh of 100 points was used for the subsequent quasi-linear computations.

Jacobs (1987) determined an analytical approximation to the $O(\epsilon)$ pressure fluctuations at the sea surface for the same logarithmic mean velocity profile, with $\nu_{wav} = \nu_{mean}[1 + O(\epsilon)]$. The $O(\epsilon)$ variations in ν_{wav} are because its gradient is assumed to be proportional to the square root of the instantaneous shear stress rather than the square root of the mean shear stress. His approximation is valid for small ϵ_J, where, neglecting z_0 in comparison with k^{-1},

$$\epsilon_J = \kappa/[\log(k^{-1}/z_0)] = U_*/U(k^{-1}) \equiv [C_D(k^{-1})]^{1/2} \tag{3.1}$$

is the square root of the drag coefficient referred to a height of k^{-1}. His expression for the component of the pressure fluctuation in phase with the surface slope is

$$\mathrm{Im}\check{p}_k = 2\kappa\epsilon_J\left[\frac{U(k^{-1}) - c_p}{U(k^{-1})}\right]\left[\frac{U(k^{-1})}{c_p}\right]^2 = 2\kappa U_*[U(k^{-1}) - c_p]/c_p^2. \tag{3.2}$$

A plot of the ratio of the linear model result for $\mathrm{Im}\check{p}_k$ (with 1000 mesh points and $f = 0.2$ Hz) to that obtained from (3.2), for 11 values of ϵ_J and three values of $U(k^{-1})/c_p$, is shown in Fig. 1. The linear model gives generally higher values than Jacobs' expression, but the ratio tends to unity as ϵ_J is reduced. The discrepancies that arise for $\epsilon_J = 0.01$ are due to rounding or truncation errors in the numerical scheme: z_0 is then less than 10^{-16} m.

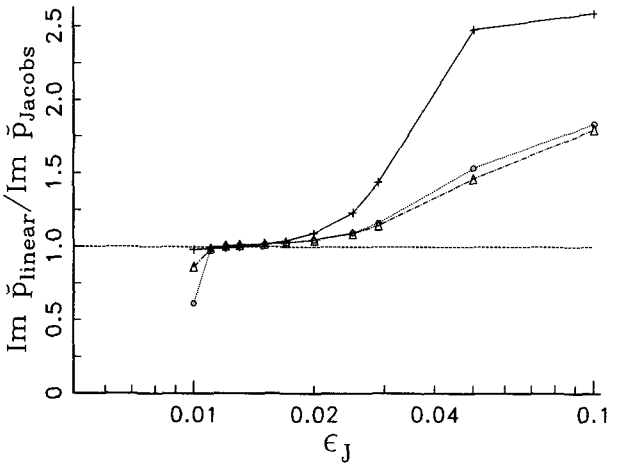

FIG. 1. Ratio of the pressure fluctuation contribution to wave-energy input for the linear model to that obtained by Jacobs (1987), as a function of $\epsilon_J = U_*/U(k^{-1})$. Solid line with crosses: $U(k^{-1})/c_p = 2$. Dotted line with circles: $U(k^{-1})/c_p = 5$. Dash-dotted line with triangles: $U(k^{-1})/c_p = 10$.

b. *Quasi-linear model*

Including the nonlinear terms in the mean-flow equations and running the model iteratively for a single wave component of frequency 0.2 Hz, using 100 mesh points in a domain of height 500 m, we obtain rates of wave-energy input S_{in} from pressure and shear-stress fluctuations that are shown in Fig. 2 for an applied stress given by $\tau_w/\rho = 0.49$ m^2 s^{-2} (so $c_p/U_* = 11.15$) and a roughness length $z_0 = 0.7195$ mm (corresponding to a Charnock coefficient $\alpha = 0.0144$). The air/water density ratio is assumed to be $\rho/\rho_w = 1.25 \times 10^{-3}$. The results for the linear model are shown for comparison. The iterative method converged rather slowly: I used 1000 iterations with a relaxation parameter $\lambda = 0.05$, letting the wave amplitude increase gradually from zero during the first 500 iterations.

The graph of the rate of wave energy input as a function of wave slope or wave amplitude follows the linear model curve for small slopes, and then diverges below it, reaching a plateau at $k\tilde{\zeta}_0 \approx 0.3$. This reduction in S_{in} relative to the linear model is probably due to the reduction in mean velocity (shown in Fig. 4), the increase in the critical height $c = z_c$ at which $U(c) = c_p$, and the corresponding decrease in magnitude of the "curvature" of the mean velocity profile, $U_{cc}(z_c)/[U_c(z_c)]^3$. The semilogarithmic plot shown in Fig. 4 indicates that the effect of increasing wave slope is to reduce the wind speed by a constant amount for heights greater than z_c and to reduce the curvature of the velocity profile below that height. The decrease in mean velocity for constant τ_w means that the drag coefficient increases, as is shown in Fig. 3 for $C_D(10\text{ m})$. The momentum flux Π_{in} from the atmosphere to these monochromatic waves is proportional to the energy input shown in Fig. 2 and is 0.67 times the total air–sea momentum flux for $k\tilde{\zeta}_0 = 0.4$.

The model was then run for the continuous unidirectional wave spectra of the JONSWAP type (Hasselmann et al. 1973). The spectra have the following form:

$$F(f) = \alpha_P g^2(2\pi)^{-4} f^{-5}\gamma^\Gamma \exp\left[-\frac{5}{4}\left(\frac{f}{f_m}\right)^{-4}\right], \tag{3.3}$$

with $\Gamma = \exp[-(f - f_m)^2/(2\sigma^2 f_m^2)]$. Following Jans-

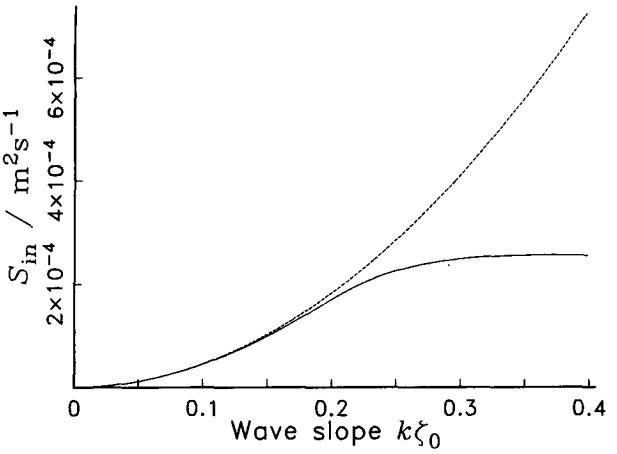

FIG. 2. Rate of energy input as a function of slope for a monochromatic wave. Solid line: quasi-linear model. Dashed line: linear model. ($U_* = 0.7$ m s^{-1}, Charnock coefficient $\alpha = 0.0144$, $c_p/U_* = 11.15$.)

sen (1989), we take $\gamma = 3.3$, $\sigma = 0.10$, and the Phillips constant $\alpha_P = 0.57[c_p(f_m)/U_*]^{-3/2}$, where $c_p(f_m) = g/(2\pi f_m)$ is the wave phase speed at the spectral peak frequency f_m, and we choose $U_* = 0.7$ m s^{-1}, as in the case of the monochromatic wave. The spectrum was discretized at equal intervals of log$f$, the lowest frequency being 0.047 Hz, the highest 9.416 Hz, and the ratio between adjacent frequencies being $e^{0.1} = 1.1052$, with a total of 54 wave components. Five different spectra were used, with the wave age $c_p(f_m)/U_*$ ranging from 5 ("young" sea state) to 25 ("old" sea state).

The computational domain was again 100 mesh points with a total vertical extent of 500 m; and 900 iterations were performed with $\lambda = 0.06$, the amplitude $\tilde{\zeta}_{k0}$ of each wave component being increased gradually from zero during the first 450 iterations.

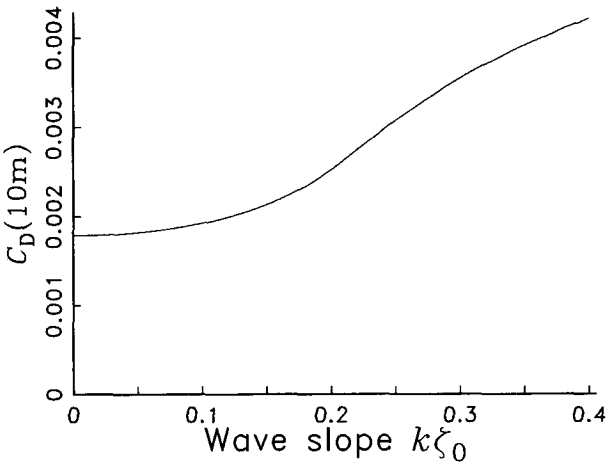

FIG. 3. Drag coefficient as a function of monochromatic wave slope. Conditions as for Fig. 2.

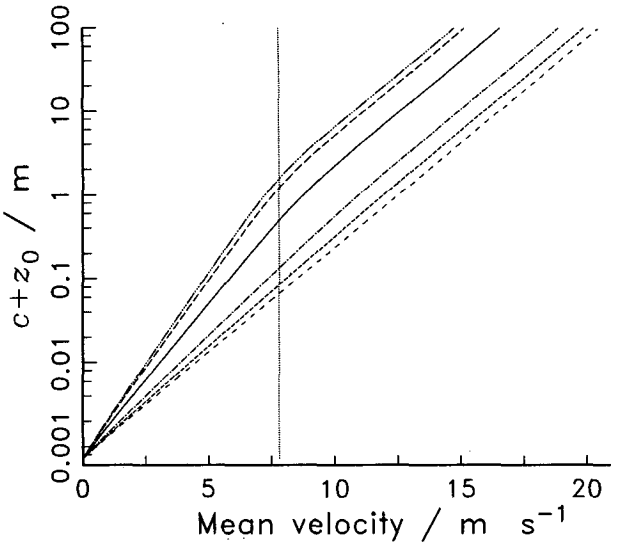

FIG. 4. Velocity profile for different monochromatic wave slopes (dotted line marks the wave phase speed). Conditions as for Fig. 2. The profiles in order of decreasing velocity are: (i) no waves (open dashed line), (ii) $k\tilde{\zeta}_0 = 0.10$, (iii) $k\tilde{\zeta}_0 = 0.16$, (iv) $k\tilde{\zeta}_0 = 0.25$ (solid line), (v) $k\tilde{\zeta}_0 = 0.35$, and (vi) $k\tilde{\zeta}_0 = 0.40$.

The resulting rate of wave energy input is shown in scaled form in Fig. 5 for $c_p(f_m) = 5$ and $c_p(f_m) = 25$, with the corresponding results of Janssen (1989) for comparison. The growth rates are generally of the same order of magnitude as those of Janssen.

The drag coefficient calculated for 10 m above the sea surface is shown in Fig. 6, together with the corresponding results for $U_* = 0.3$ m s^{-1} and for an alternative Phillips constant formulation, $\alpha_P = 0.054[c_p(f_m)/U_*]^{-2/3}$. This latter formulation for the Phillips constant gives a rather slowly varying drag coefficient, when compared with the systematic increase with decreasing wave age for the $(-3/2)$-power dependence of α_P on the wave age. The Janssen (1989) model shows a similar but more marked increase in C_D(10 m) for young sea states. The curve fitted to the North Sea experimental results of Geernaert et al. (1987) shows a very strong wave-age dependence, but this is to be expected since their results are for a wide range of U_* values, rather than a single value. In field experiments we would expect that high values of U_* would be associated with young sea states and low values with older, more fully developed seas. The present model gives drag coefficients for $U_* = 0.7$ m s^{-1} very close to those calculated by Maat et al. (1991) from analysis of the HEXMAX field data and rather higher values though still fairly close, for $U_* = 0.3$ m s^{-1}. The corresponding drag coefficients calculated from Donelan's (1982, 1990) Lake Ontario field experimental results are based on his fitted formula

$$\frac{z_{0\text{eff}}}{F^{1/2}} = 1.84\left[\frac{U_*}{c_p(f_m)}\right]^{2.53}, \qquad (3.4)$$

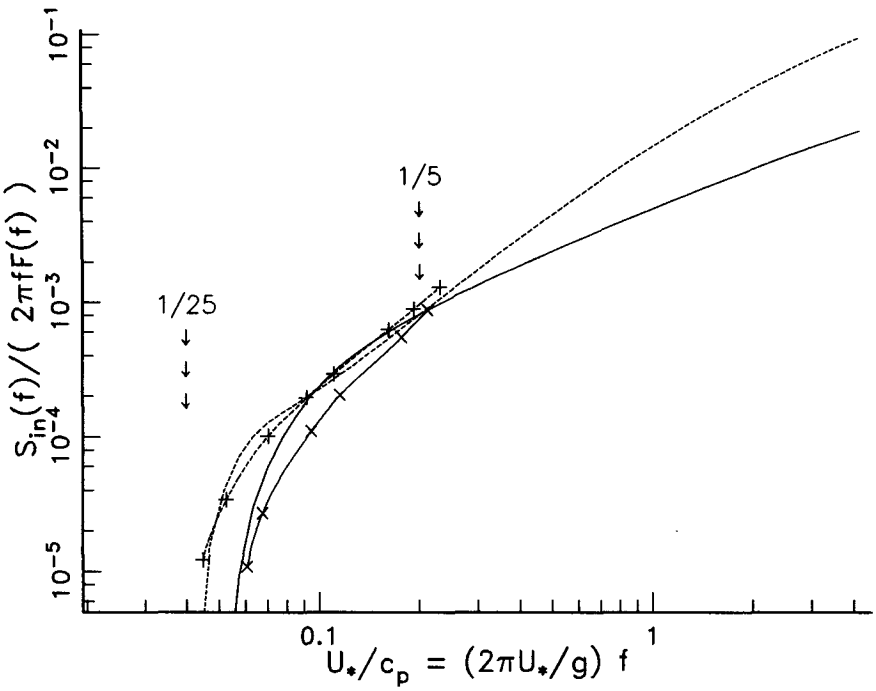

FIG. 5. Rate of wave energy input divided by spectral density and angular frequency for the quasi-linear model (lines with no symbols) and the model of Janssen (1989) (lines with symbols). JONSWAP spectra used, with Phillips constant $\alpha_P = 0.57[c_p(f_m)/U_*]^{-3/2}$ and $U_* = 0.7$ m s^{-1}. Solid lines: $c_p(f_m)/U_* = 5$ ("young" sea: "1/5" marks the spectral peak frequency f_m); the plain line is the quasi-linear model; crosses mark Janssen's results; Dashed lines: $c_p(f_m)/U_* = 25$ ("old" sea: "1/25" marks the spectral peak frequency f_m); the plain line is a quasi-linear model, plus signs mark Janssen's results.

where F is the mean-square surface displacement due to the waves, and $z_{0\text{eff}}$ is the "effective roughness length" given by the wind velocity profile, so that $C_D(10\text{ m}) = [\kappa/\log(10\text{ m}/z_{0\text{eff}})]^2$. The present model, Janssen's (1989), and the Maat et al. (1991) analysis give drag coefficients somewhat greater than these results from Donelan.

Figure 7 shows the momentum flux from the atmosphere to the wave field, determined by (1.8), divided by the total momentum flux ρU_*^2. For the present quasi-linear model, the waves account for between 0.26 and 0.89 of the total momentum flux when $5 \leq c_p(f_m)/U_* \leq 25$, $U_* = 0.7$ m s^{-1}, and $\alpha_P \propto [c_p(f_m)/U_*]^{-3/2}$, the range of variation being considerably smaller for the $(-2/3)$-power dependence. In Janssen's quasi-linear model, when $U_* = 0.7$ m s^{-1} and $\alpha_P \propto [c_p(f_m)/U_*]^{-3/2}$, the waves account for between 0.36 and 0.94 of the total momentum flux, the difference from the present model being rather large for $c_p(f_m)/U_*$ in the middle of the range (between about 10 and 20).

I have also plotted the ratio of wave to total momentum flux which was calculated from the published values of S_{in}, obtained by Makin and Chalikov (Chalikov 1986b, Fig. 11c) using a turbulence closure model in curvilinear coordinates for the airflow over sea surfaces with simulated JONSWAP wave spectra. These values are considerably smaller than the other results, perhaps because the authors used a more limited spectral range for the wave Fourier components. Their model had a ratio of maximum to minimum frequency of about 6 and a maximum frequency of about three times the spectral peak frequency, whereas the present model has corresponding frequency ratios of 200 and at least 20.

Makin (1987) also calculated various contributions to the momentum flux over a sea surface with a "developed" Pierson–Moskowitz spectrum and obtained a momentum flux associated with the wave-induced air motions of $\sim$0.154 times the total momentum flux. The drag coefficient at the top of his computational domain was specified as 1×10^{-3}, considerably smaller than the values calculated by this paper's quasi-linear model.

The contributions to air–sea momentum flux from the individual terms in (2.16) are shown as a function of the vertical coordinate c in Fig. 8 for $U_* = 0.7$ m s^{-1}, $c_p(f_m)/U_* = 5$, and $\alpha_P \propto [c_p(f_m)/U_*]^{-3/2}$. At the sea surface, the nonzero terms are $\overline{\tau}_{13}$, $\overline{p'\zeta_a}$, $-\overline{\tau'_{11}\zeta_a}$ and $\overline{\tau'_{13}\xi_a}$. The last two terms are relatively small and of opposite sign at the surface, so the pressure–slope correlation does provide the major contribution to the

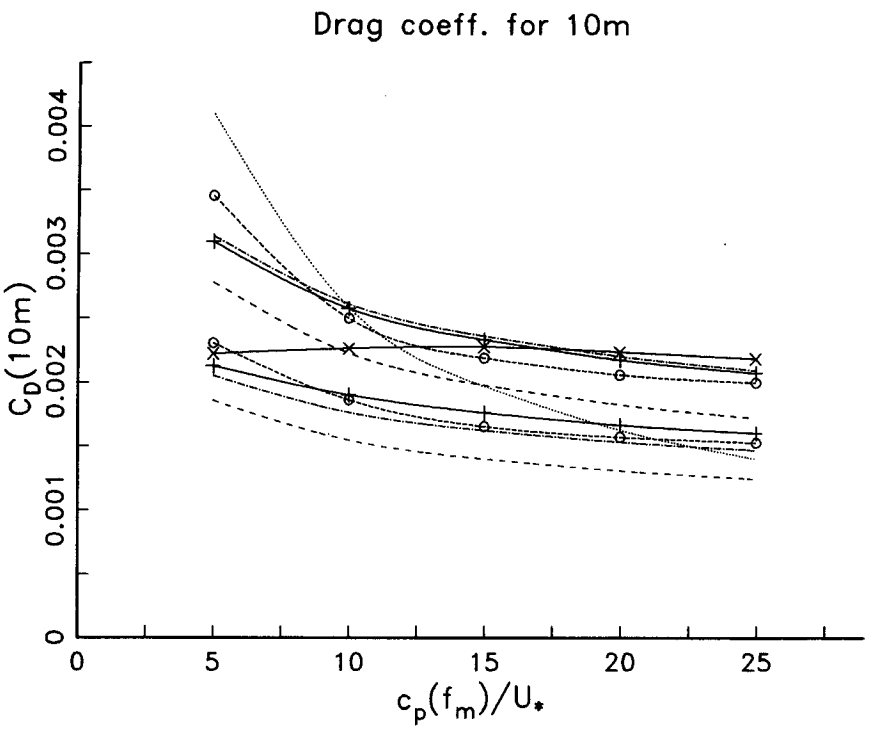

FIG. 6. Drag coefficient as a function of wave age. Solid lines: quasi-linear model for JONSWAP spectra. (Solid lines with plus signs: $\alpha_P = 0.57[c_p(f_m)/U_*]^{-3/2}$. Upper curve, $U_* = 0.7$ m s^{-1}. Lower curve, $U_* = 0.3$ m s^{-1}.) (Solid line with crosses: $\alpha_P = 0.054[c_p(f_m)/U_*]^{-2/3}$, $U_* = 0.7$ m s^{-1}.) Close dashed lines with circles: Janssen's (1989) model for JONSWAP spectra and $\alpha_P = 0.57[c_p(f_m)/U_*]^{-3/2}$. (Upper curve, $U_* = 0.7$ m s^{-1}, lower curve, $U_* = 0.3$ m s^{-1}.) Dash-dotted lines: drag coefficients obtained from the analysis of HEXMAX field data by Maat et al. (1991). (Upper curve, $U_* = 0.7$ m s^{-1}, lower curve, $U_* = 0.3$ m s^{-1}.) Open dashed lines: drag coefficients obtained from the analysis of Lake Ontario data by Donelan (1990). (Upper curve, $U_* = 0.7$ m s^{-1}, lower curve, $U_* = 0.3$ m s^{-1}.) Dotted line: the curve fitted by Geernaert et al. (1987) to North Sea experimental results with a range of values of U_*.

wind-to-wave momentum and energy flux. The mean shear stress $\bar{\tau}_{13}$, averaged with respect to the curvilinear coordinate system, is equal to τ_w at the top of the domain and decreases to $0.17\tau_w$ at the sea surface, the wave-correlated terms carrying the rest of the momentum flux. The corresponding profile of mean wind velocity U is shown in Figs. 9 (logarithmic vertical scale) and 10 (linear vertical scale). The logarithmic-scale graph shows the transition from a logarithmic velocity profile to one that has a reduced curvature as the sea surface is approached; and the linear-scale graph shows that the second derivative of the velocity profile is everywhere negative.

The fluctuating shear-stress contribution to wave energy input, via the term $\overline{\tau'_{13}\xi_t}$ in (2.41), gives rise to a wind-to-wave momentum flux of $-\overline{\tau'_{13}\xi_a}$. For $c_p(f_m)/U_* = 5$, $\alpha_P \propto [c_p(f_m)/U_*]^{-3/2}$, this is $\approx 0.08\tau_w$. In a laboratory wave-tank study, Okuda et al. (1977) determined the variation of the shear stress over wind-wave profiles by measuring the velocity shear in the water just below the surface. Their results indicate that $-\overline{\tau'_{13}\xi_a}$ is greater than $0.2\tau_w$, much greater than the value calculated here. However, in their experiment the wave age was $c_p/U_* \approx 0.75$, a very small value, and their waves were very steep. Thus, we can expect their experiment to show very vigorous flow separation and consequently a large shear-stress fluctuation.

4. Discussion

The model described in this report calculates the flow field in the boundary layer above the sea surface using the quasi-linear approximation in conjunction with a curvilinear coordinate system where one of the coordinate surfaces coincides with the instantaneous sea surface. From the flow field parameters, the rate of energy input to the waves can be calculated. Although a more complete description of the airflow above the waves can in principle be obtained by a direct Monte Carlo simulation of the movements of the water surface (e.g., Makin 1980, 1987), the quasi-linear approximation does include the $O(\epsilon^2)$ effects of the wave motions on the mean flow-field properties, and should be less expensive computationally. It ensures momentum

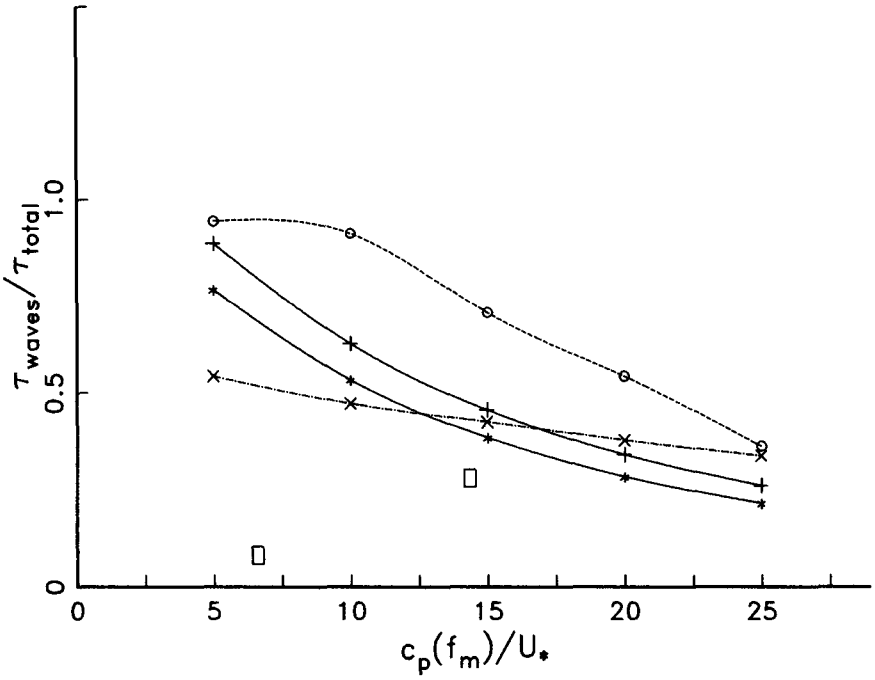

FIG. 7. Ratio of wind-to-wave momentum flux to total momentum flux, as a function of wave age for JONSWAP spectra. Solid lines: quasi-linear model, $\alpha_P \propto [c_p(f_m)/U_*]^{-3/2}$. (Solid line with plus signs: $U_* = 0.7$ m s^{-1}. Solid line with asterisks: $U_* = 0.3$ m s^{-1}.) Dashed line with circles: Janssen's (1989) model with $U_* = 0.7$ m s^{-1} and $\alpha_P \propto [c_p(f_m)/U_*]^{-3/2}$. Dash-dotted line with crosses: quasi-linear model, $U_* = 0.7$ m s^{-1} and $\alpha_P \propto [c_p(f_m)/U_*]^{-2/3}$. Rectangles: turbulence closure model of Chalikov and Makin (Chalikov 1986b Fig. 11c).

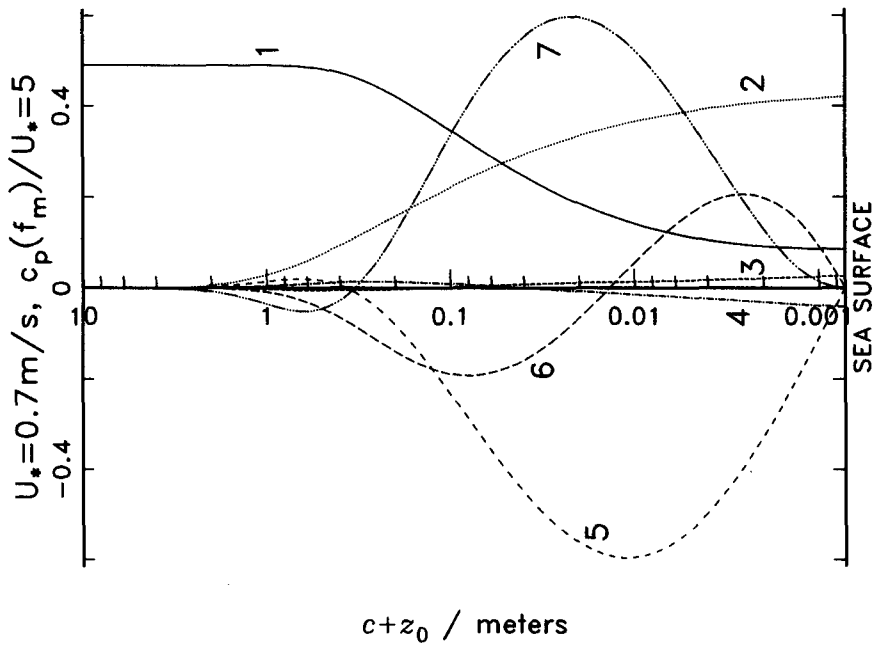

FIG. 8. Vertical profile of the various contributions to the downward momentum flux, calculated by the quasi-linear model [see (2.16).] Friction velocity $U_* = 0.7$ m s^{-1}, JONSWAP wave spectrum with $\alpha_P \propto [c_p(f_m)/U_*]^{-3/2}$ and $c_p(f_m)/U_* = 5$. The sea surface is at the bottom of the plot, where $c + z_0 = z_0$; here, $z_0 = 0.720$ mm from (2.26). The numbers on the graphs refer to the different terms of (2.19), as follows: 1, $\bar{\tau}_{13}/\rho$; 2, $\overline{p'\zeta_a}/\rho$; 3, $-\overline{\tau'_{11}\zeta_a}/\rho$; 4, $\overline{\tau'_{13}\xi_a}/\rho$; 5, $\overline{u'\zeta_t}$; 6, $-\overline{u'w'}$; 7, $U\overline{u'\zeta_a}$.

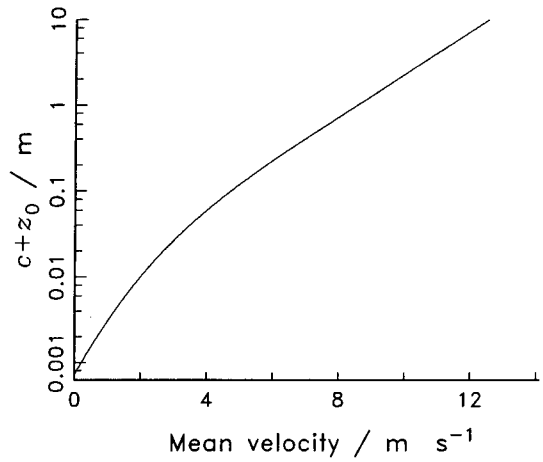

FIG. 9. Profile of the mean wind velocity (logarithmic scale of height). Same conditions as for Fig. 8.

conservation, in the sense that the wind-to-wave momentum flux associated with the energy input to the waves from the wind never exceeds the amount available from the applied wind stress.

The curvilinear coordinate system enables rapid vertical variations of mean-flow parameters to be resolved in the region just above the sea surface. It does, however, require one to solve rather complicated equations, particularly when the effect of viscosity (or turbulent Reynolds stress) is incorporated. Consequently, a simplified form is adopted for the parameterization of the stresses due to turbulent motions and viscosity. Since the effect of turbulent motions on mean momentum transport is imperfectly known, particularly in the presence of a moving boundary, such a simplified parameterization may be justified.

The model equations are solved iteratively on a vertical one-dimensional logarithmically spaced finite-difference mesh. A linear version of the model gave results in agreement with those produced by Conte and Miles' (1959) numerical solution of the Rayleigh equation if a very small "wave" total viscosity (Newtonian viscosity plus eddy viscosity) was used, in spite of the fact that no-slip boundary conditions were used at the sea surface. Rates of wave energy input for the linear model are generally greater than those of the analytical eddy-viscosity model of Jacobs (1987) but converge to them if the roughness length becomes very small. These comparisons indicate that the linear numerical model has correct mathematical behavior.

When the model was then run in nonlinear (quasi-linear) mode with a constant applied wind stress over a monochromatic wave, as the wave amplitude was increased, the mean air velocity decreased. The effective drag coefficient thus increased with wave amplitude. The ratio of the rate of energy input calculated by the quasilinear model to the rate calculated by an equivalent linear model decreased—the energy input rate reaching a plateau for a wave slope $k\tilde{\zeta}_0 \approx 0.3$. The waves thus increase the effective surface roughness, reducing the mean airspeed, momentum being transferred to the ocean by means of increased pressure on the upwind slopes of the waves.

Wind-wave sea states with JONSWAP spectra were simulated using 54 logarithmically spaced unidirectional wave Fourier components. Generally speaking, a large number of iterations was required for convergence (around 900 for a 100-point mesh). There is thus obvious room for improvement in the numerical techniques used. Fixed values of 0.7 and 0.3 m s^{-1} were used for the friction velocity U_*, and the wave age $c_p(f_m)/U_*$ was varied from 5 to 25. Rates of wave energy input were in general agreement with those calculated by Janssen's (1989) simpler quasi-linear model. The wave energy input is primarily due to the component of the pressure fluctuation in phase with the surface slope. The contributions of the fluctuating viscous and Reynolds stresses (τ'_{11}, τ'_{33} and τ'_{13}) are considerably smaller. If the Phillips constant α_P of the wave spectrum is made proportional to the $(-3/2)$ power of the wave age, the waves affect the mean air velocity in such a way that the drag coefficient $C_D(10\text{ m})$ is a decreasing function of wave age. This is in agreement with Janssen's model, though the present model gives a somewhat slower rate of decrease than Janssen's. It disagrees with calculations performed by Nordeng (1991), based on the moving-roughness-element theory of Kitaigorodskii (1973) and empirical expressions for $S_{in}(f)$, which predict a maximum in C_D for $c_p(f_m)/U_* \approx 10$.

In comparison with analyses of field experimental results for the dependence of drag coefficient on wave age, the present model's results are in rather good agreement with those of Maat et al. (1991), and greater

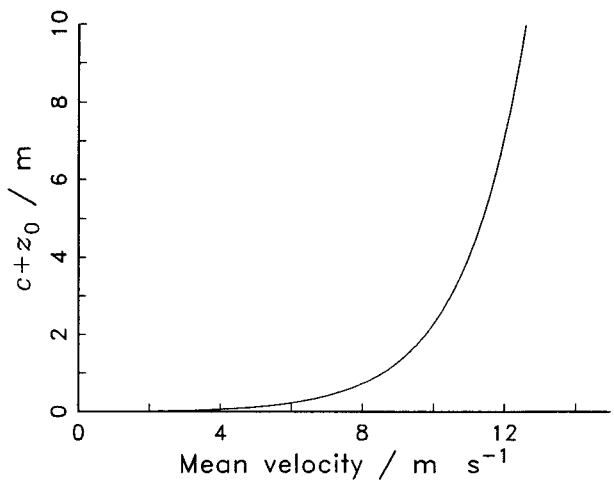

FIG. 10. Profile of the mean wind velocity (linear scale of height). Same conditions as for Fig. 8.

than, though parallel to, those of Donelan (1990). The drag coefficients calculated by Geernaert et al. (1987) vary much more rapidly with wave age, but they give a single curve for a whole range of values of U_*, and their observed U_* values can be expected in general to decrease with increasing wave age. The model disagrees with the analysis of field and laboratory data by Toba et al. (1990), in which the effective roughness length and drag coefficient increase with wave age, instead of decreasing.

When the quasilinear model was run with the Phillips constant α_P proportional to the $(-2/3)$ power of wave age, the drag coefficient became a much more slowly varying function of wave age, with a maximum at $c_p(f_m)/U_* \approx 17.5$.

The ratio of the wind-to-wave momentum flux to the total wind stress varies from about 0.9 to about 0.25 as $c_p(f_m)/U_*$ varies from 5 to 25, for $\alpha_P \propto [c_p(f_m)/U_*]^{-3/2}$ and $U_* = 0.7$ m s^{-1}. The corresponding figures for the Janssen (1989) model are 0.95 and 0.35. For $c_p(f_m)/U_*$ between 10 and 20, the present model gives a significantly lower ratio than Janssen's model. The ratios are higher than those calculated by the turbulence closure model of Chalikov and Makin (Chalikov 1986b; Makin 1987), probably because of the present model's greater spectral range.

The dominant contribution to wave energy input is the pressure–slope correlation. The contribution of the fluctuating shear stress τ'_{13} is considerably smaller, even for steep wind seas with $U_* = 0.7$ m s^{-1}, $\alpha_P = 0.57[c_p(f_m)/U_*]^{-3/2}$, and $c_p(f_m)/U_* = 5$, when it accounts for about 8% of the air–sea momentum flux. The large values of fluctuating shear stress, accounting for over 20% of the air–sea momentum flux, which were obtained in the laboratory experiment of Okuda et al. (1977), are probably a result of the very low wave age ($c_p/U_* \approx 0.75$) in their experimental run.

The quasi-linear model described here should be capable of substantial improvement. It should be straightforward to extend the analysis to three dimensions in order to apply it to directionally spread wave spectra. The behavior of the Reynolds stress components is an obvious area for further investigation and comparison with observations. The numerical techniques need to be improved to attain more rapid convergence: it should be possible to use a coarser mesh near the surface and parameterize analytically the region between the lowest mesh point and the true sea surface (Chalikov 1978, 1986b). The influence of wave breaking—a strongly nonlinear process—on wave generation, obviously cannot be included directly in this $O(\epsilon^2)$ perturbation formulation, but it may be possible to include its effect in an empirical manner, using experimental results (Banner 1990) and other types of theoretical analysis (Csanady 1990). The same can probably be said for the influence of three-dimensional airflow patterns above the waves (Stewart 1974; Csanady 1985).

Acknowledgments. I would like to thank numerous people for valuable comments, suggestions, and discussions, particularly Bjørn Ådlandsvik, Trond Aukrust, Michael Banner, Fred Dobson, Mark Donelan, Peter Janssen, Anne Karin Magnusson, Martin Mork, Thor Erik Nordeng, Will Perrie, Magnar Reistad and Stu Smith. I am also grateful for constructive comments by two anonymous referees that led to substantial improvements in this manuscript.

REFERENCES

Al-Zanaidi, M. A., and W. H. Hui, 1984: Turbulent airflow over water waves—a numerical study. *J. Fluid Mech.*, **148,** 225–246.

Anderson, J. L., S. Preiser, and E. L. Rubin, 1968: Conservation form of the equations of hydrodynamics in curvilinear coordinate systems. *J. Comput. Phys.*, **2,** 279–287.

Andrews, D. G., and M. E. McIntyre, 1978: An exact theory of nonlinear waves on a Lagrangian-mean flow. *J. Fluid Mech.*, **89,** 609–646.

Banner, M. L., 1990: The influence of wave breaking on the surface pressure distribution in wind–wave interactions. *J. Fluid Mech.*, **211,** 463–495.

Brooke Benjamin, T., 1959: Shearing flow over a wavy boundary. *J. Fluid Mech.*, **6,** 161–205.

Caponi, E. A., B. Fornberg, D. D. Knight, J. W. McLean, P. G. Saffman, and H. C. Yuen, 1982: Calculations of laminar viscous flow over a moving wavy surface. *J. Fluid Mech.*, **124,** 347–362.

Chalikov, D. V., 1978: The numerical simulation of wind–wave interaction. *J. Fluid Mech.*, **87,** 561–582.

——, 1986a: Spectrum of energy flux to waves. *Oceanology,* **26,** 145–148. (Engl. transl.)

——, 1986b: Numerical simulation of the boundary layer above waves. *Bound.-Layer Meteor.*, **34,** 63–98.

Chang, M.-S., 1969: Mass transport in deep-water long-crested random gravity waves. *J. Geophys. Res.*, **74,** 1515–1536.

Charnock, H., 1955: Wind stress on a water surface. *Quart. J. Roy. Meteor. Soc.*, **81,** 639–640.

Conte, S. D., and J. W. Miles, 1959: On the numerical integration of the Orr–Sommerfeld equation. *J. Soc. Indust. Appl. Math.*, **7,** 361–366.

Craik, A. D. D., 1982: The generalized Lagrangian-mean equations and hydrodynamic stability. *J. Fluid Mech.*, **125,** 27–35.

Croft, A. J., and S. G. Sajjadi, 1990: An improved theory of the Miles–Benjamin mechanism applied to Stokes waves. *Proc. Roy. Soc. London,* **A,** in press.

Csanady, G. T., 1985: Air–sea momentum transfer by means of short-crested wavelets. *J. Phys. Oceanogr.*, **15,** 1486–1501.

——, 1990: Momentum flux in breaking wavelets. *J. Geophys. Res.*, **95,** 13 289–13 299.

Donelan, M., 1982: The dependence of the aerodynamic drag coefficient on wave parameters. *First Int. Conf. on Meteorology and Air–Sea Interaction of the Coastal Zone.* de Bilt, Amer. Meteor. Soc., 381–387.

——, 1990: Air–sea interaction. *The Sea,* Vol. 9, B. LeMehaute and D. Hines, Eds., Wiley, 239–292.

Eiseman, P. R., and A. P. Stone, 1980: Conservation laws of fluid dynamics—A survey. *SIAM Rev.*, **22,** 12–27.

Fabrikant, A. L., 1976: Quasilinear theory of wind-wave generation. *Izv. Atmos. Ocean. Phys.*, **12,** 524–526. (Engl. transl.).

Geernaert, G., S. E. Larsen, and F. Hansen, 1987: Measurements of the wind stress, heat flux, and turbulence intensity during storm conditions over the North Sea. *J. Geophys. Res.*, **92,** 13 127–13 139.

Gent, P. R., and P. A. Taylor, 1976: A numerical model of the air flow above water waves. *J. Fluid Mech.*, **77,** 105–128.

Gerstner, F., 1804: Theorie der Wellen. *Abhandlungen der k. böhmischen Gesellschaft der Wissenschaften,* Prague, 65 pp.

Hasselmann, K., 1962: On the non-linear energy transfer in a gravity-wave spectrum. Part 1: General theory. *J. Fluid Mech.*, **12**, 481–500.

——, 1974: On the spectral dissipation of ocean waves due to white capping. *Bound.-Layer Meteor.*, **6**, 107–127.

——, T. P. Barnett, E. Bouws, H. Carlson, D. E. Cartwright, K. Enke, J. A. Ewing, H. Gienapp, D. E. Hasselmann, P. Kruseman, A. Meerburg, P. Müller, D. J. Olbers, K. Richter, W. Sell, and H. Walden, 1973: Measurements of wind-wave growth and swell decay during the Joint North Sea Wave Project (JONSWAP). *Dtsch. Hydrogr. Z.*, **A8**(Suppl.), No. 12, 1–95.

Hsiao, S. V., and O. H. Shemdin, 1983: Measurements of wind velocity and pressure with a wave follower during MARSEN. *J. Geophys. Res.*, **88**, 9841–9849.

Hsu, C.-T., H.-Y. Wu, E.-Y. Hsu, and R. L. Street, 1982: Momentum and energy transfer in wind generation of waves. *J. Phys. Oceanogr.*, **12**, 929–951.

Jacobs, S. J., 1987: An asymptotic theory for the turbulent flow over a progressive water wave. *J. Fluid Mech.*, **174**, 69–80.

Janssen, P. A. E. M., 1982: Quasilinear approximation for the spectrum of wind-generated water waves. *J. Fluid Mech.*, **117**, 493–506.

——, 1989: Wave-induced stress and the drag of air flow over sea waves. *J. Phys. Oceanogr.*, **19**, 745–754.

——, P. Lionello, and L. Zambresky, 1989: On the interaction of wind and waves. *Phil. Trans. Roy. Soc. London*, **A329**, 289–301.

Jeffreys, H., 1925: On the formation of water waves by wind. *Proc. Roy. Soc. London*, **A107**, 189–206.

Jenkins, A. D., 1987: Wind and wave-induced currents in a rotating sea with depth-varying eddy viscosity. *J. Phys. Oceanogr.*, **17**, 938–951.

Kitaigorodskii, S. A., 1973: *The Physics of Air–Sea Interaction.* (Engl. transl.), Israel Program for Scientific Translations, 237 pp.

Knight, D., 1977: Turbulent flow over a wavy boundary. *Bound.-Layer Meteor.*, **11**, 205–222.

Lamb, H., 1932: *Hydrodynamics*, 6th ed. Cambridge University Press, 738 pp.

Lee, F. A., 1972: Some nonlinear aspects of wind–wave interactions. *J. Phys. Oceanogr.*, **2**, 432–438.

Liu, A.-K., and S. H. Davis, 1977: Viscous attenuation of mean drift in water waves. *J. Fluid Mech.*, **81**, 63–84.

Longuet-Higgins, M. S., 1953: Mass transport in water waves. *Phil. Trans. Roy. Soc. London*, **A245**, 535–581.

Maat, N., C. Kraan, and W. A. Oost, 1991: The roughness of wind waves. *Bound.-Layer Meteorol.*, **54**, 89–103.

McIntyre, M. E., 1981: On the 'wave momentum' myth. *J. Fluid Mech.*, **106**, 331–347.

Majda, A., 1984: *Compressible Fluid Flow and Systems of Conservation Laws in Several Space Variables*, Springer, 159 pp.

Makin, V. K., 1980: Numerical simulation of the structure of the near water atmospheric layer in the presence of a developed sea. *Oceanology*, **20**, 139–142. (Engl. transl.)

——, 1982: Numerical studies of wind–wave interaction. *Oceanology*, **22**, 525–530. (Engl. transl.)

——, 1987: Wavelike momentum fluxes in boundary layer above sea waves. *Oceanology*, **27**, 128–132. (Engl. transl.)

——, and Ye. G. Panchenko, 1986: Numerical studies of energy transfer from the wind to wind waves along a limited fetch. *Izv. Atmos. Ocean. Phys.*, **22**, 163–165. (Engl. transl.)

Miles, J. W., 1957: On the generation of surface waves by shear flows. *J. Fluid Mech.*, **3**, 185–204.

——, 1959: On the generation of surface waves by shear flows. Part 2. *J. Fluid Mech.*, **6**, 568–582.

——, 1960: On the generation of surface waves by turbulent shear flows. *J. Fluid Mech.*, **7**, 469–478.

——, 1962: On the generation of surface waves by shear flows. Part 4. *J. Fluid Mech.*, **13**, 433–448.

——, 1965: A note on the interaction between surface waves and wind profiles. *J. Fluid Mech.*, **22**, 823–827.

Mitsuyasu, H., and T. Honda, 1982: Wind-induced growth of water waves. *J. Fluid Mech.*, **123**, 425–442.

Navon, I. M., 1983: Conservation laws in fluid dynamics and the enforcement of their preservation in numerical discretizations. *Numerical Solution of Partial Differential Equations: Theory, Tools and Case Studies*, D. P. Laurie, Ed. Birkhäuser, 286–341.

Nordeng, T. E., 1991: On the wave age-dependent drag coefficient and roughness length at sea. *J. Geophys. Res.*, **96**(C4), 7167–7174.

Okuda, K., S. Kawai, and Y. Toba, 1977: Measurement of skin friction distribution along the surface of wind waves. *J. Oceanogr. Soc. Japan*, **33**, 190–198.

Phillips, O. M., 1960: On the dynamics of unsteady gravity waves of finite amplitude. Part I. The elementary interactions. *J. Fluid Mech.*, **9**, 193–217.

Pierson, W. J., 1961: Models of random seas based on the Lagrangian equations of motion. Technical Report prepared for the Office of Naval Research under Contract Nonr-285(03) 39 pp. [Available from the College of Engineering, Research Division, New York University.]

Plant, W. J., 1982: A relationship between wind stress and wave slope. *J. Geophys. Res.*, **87**, 1961–1967.

Pollard, R., 1973: Interpretation of near-surface current meter observations. *Deep-Sea Res.*, **20**, 261–268.

Prandtl, L., 1925: Bericht über Untersuchungen zur ausgebildeten Turbulenz. *Z. angew. Math. Mech.*, **5**, 136–139.

Sajjadi, S. G., 1988: Shearing flows over Stokes waves. 234 pp. [Report available from the Coventry Polytechnic, Priory St., Coventry, CV1 5FB, England.]

Shyy, W., and T. C. Vu, 1991: On the adoption of velocity variable and grid system for fluid flow computation in curvilinear coordinates. *J. Comput. Phys.*, **92**, 82–105.

Snyder, R. L., F. W. Dobson, J. A. Elliott, and R. B. Long, 1981: Array measurements of atmospheric pressure fluctuations above surface gravity waves. *J. Fluid Mech.*, **102**, 1–59.

Stewart, R. W., 1961: The wave drag of wind over water. *J. Fluid Mech.*, **10**, 189–194.

——, 1974: The air–sea momentum exchange. *Bound.-Layer Meteor.*, **6**, 151–167.

Stokes, G. G., 1847: On the theory of oscillatory waves. *Trans. Cambridge Phil. Soc.*, **8**, 441–455.

The SWAMP Group, 1985: *Ocean Wave Modelling.* Plenum, 256 pp.

Taylor, P. A., and P. R. Gent, 1978: A numerical investigation of variations in the drag coefficient for air flow above water waves. *Quart. J. Roy. Meteor. Soc.*, **104**, 979–988.

Toba, Y., N. Iida, H. Kawamura, N. Ebuchi, and I. S. F. Jones, 1990: Wave dependence of sea-surface wind stress. *J. Phys. Oceanogr.*, **20**, 705–721.

Townsend, A. A., 1972: Flow in a deep turbulent boundary layer over a surface distorted by water waves. *J. Fluid Mech.*, **55**, 719–735.

Vinokur, M., 1974: Conservation equations of gasdynamics in curvilinear coordinate systems. *J. Comput. Phys.*, **14**, 105–125.

Weber, J. E., 1983: Steady wind- and wave-induced currents in the open ocean. *J. Phys. Oceanogr.*, **13**, 524–530.

——, 1990: Eulerian versus Lagrangian approach to wave drift in a rotating ocean. *Kung. Vetenskaps- og Vitterhets-Samhället, Göteborg, Acta: Geophysica*, **3**, 155–170.